Environmental Research 201 (2021) 111596

Contents lists available at ScienceDirect

Environmental Research

journal homepage: www.elsevier.com/locate/envres

Robust Cr(VI) reduction over hydroxyl modified UiO-66 photocatalyst constructed from mixed ligands: Performances and mechanism insight with or without tartaric acid

Yu-Hang Li [a], Xiao-Hong Yi [a], Yu-Xuan Li [a], Chong-Chen Wang [a,*], Peng Wang [a], Chen Zhao [a], Weiwei Zheng [b]

[a] Beijing Key Laboratory of Functional Materials for Building Structure and Environment Remediation, School of Environment and Energy Engineering, Beijing University of Civil Engineering and Architecture, Beijing, 100044, China
[b] Department of Chemistry, Syracuse University, Syracuse, NY, 13244, United States

ARTICLE INFO

Keywords:
UiO-66
Hydroxyl groups
Tartaric acid
Hexavalent chromium
Photocatalytic reduction

ABSTRACT

Hydroxyl modified UiO-66 ($(OH)_2$-UiO-66-X%, X represents the mass content ratio of introduced 2,5-dihydroxyterephthalic acid) was prepared via a solvothermal reaction between zirconium tetrachloride, benzene-1,4-dicarboxylic acid (H_2BDC), as well as 2,5-dihydroxyterephthalic acid (H_2BDC-$(OH)_2$). It was found that hydroxyl groups can act as the intramolecular hole scavenger to boost the photo-induced charge carrier separation to enhance Cr(VI) reduction. The photocatalytic Cr(VI) reduction activities of $(OH)_2$-UiO-66-X% were investigated upon the irradiation of low-power ultraviolet LED light. The findings demonstrated that $(OH)_2$-UiO-66-20% with good cyclicity and stability exhibited superior photocatalytic performances to both UiO-66 and $(OH)_2$-UiO-66. The introduction of hydroxyl groups can also extend the light absorption region to longer wavelength in visible range, which provides possibility for displaying photocatalytic activities under sunlight. The effect of small molecule organic acid (SOAs), pH value, and co-existing inorganic ions on photocatalytic performances of $(OH)_2$-UiO-66-20% were investigated. Tartaric acid (TA) as typical SOAs was introduced to the reaction system to further boost the photocatalytic Cr(VI) reduction via acting as hole scavenger, constructing charge-transfer-complex for quick electron transportation, and producing $COO^{\cdot-}$ radicals. This work opened a new opportunity for modified MOFs for boosted elimination activities for environmental pollutants.

1. Introduction

For many years, the development of industrialization has been accompanied by the disposal of various heavy metal pollutants into the environment (Karnitz et al., 2007). These heavy metal ions including chromium (especially hexavalent chromium), lead, mercury, nickel, and copper are toxic and can exert potential threats to ecology and creatures (Owlad et al., 2009; Du et al., 2020). Among them, hexavalent chromium, Cr(VI), is extremely toxic, which can exert threat to the human health via digestion, respiratory tract, skin and mucosa (Wang et al., 2016a; Shen et al., 2019). Generally, Cr(VI) was discharged in the wastewater from different industries like electroplating, chromate leather tanning along with paint-making (Owlad et al., 2009; Wang et al., 2016a; Huang et al., 2017; Testa et al., 2004; Chen et al., 2019). Some technologies including ion exchange (Xing et al., 2007), membrane separation (Liu et al., 2020a), adsorption (Lu et al., 2016), and electrocoagulation (Heidmann and Calmano, 2008) have been used to remove Cr(VI) from wastewater. Reducing toxic Cr(VI) to less toxic Cr (III) was deemed as the preferrable approach of Cr(VI) elimination (Huang et al., 2017; Liang et al., 2015), due to that Cr(III) can be facilely precipitated into solid $Cr(OH)_3$. In recent years, there are increasing attentions on photoreduction of Cr(VI) into Cr(III) in wastewater treatment (Zhang et al., 2018a, 2019), considering that photocatalysis is effective, low-cost and free of secondary hazardous chemicals.

As highly porous materials constructed from metal templates and organic linkers, metal-organic frameworks (MOFs) were already used as functional environment materials in various fields like sensing, adsorption, antibacterial and advanced oxidation processes (photocatalysis, photo-Fenton, persulfate activation) (Li et al., 2020a; Yi et al., 2021; Xiong et al., 2020; Huang et al., 2021; Peng et al., 2018; Yi and

* Corresponding author.
E-mail addresses: wangchongchen@bucea.edu.cn, chongchenwang@126.com (C.-C. Wang).

https://doi.org/10.1016/j.envres.2021.111596
Received 18 May 2021; Received in revised form 6 June 2021; Accepted 22 June 2021
Available online 2 July 2021

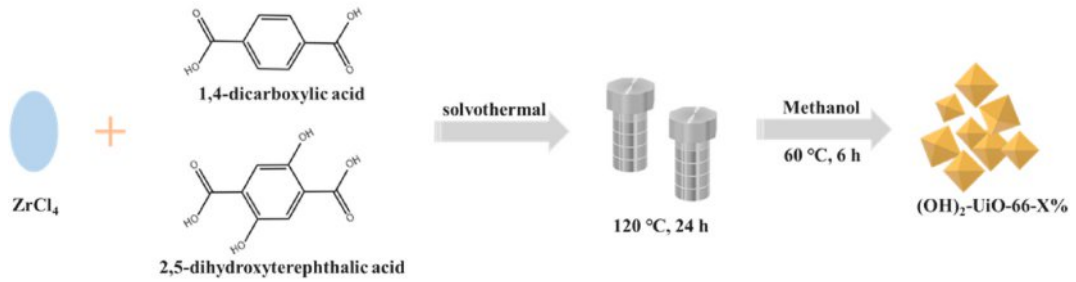

Scheme 1. Diagrammatic fabrication sketch of series $(OH)_2$-UiO-66-X% via solvothermal method.

Wang, 2021; Liu et al., 2018; Wang et al., 2019). UiO-66 (Zirconium 1, 4-dicarboxybenzene), one of the typical MOFs, attracted extensive attentions, considering its ultrahigh surface area and good chemical/thermal stability (Cavka et al., 2008; Wu et al., 2013; Wiersum et al., 2011; Valenzano et al., 2011; Fu-Xue et al., 2017). However, the pristine UiO-66 demonstrated poor photocatalytic performances due to its limited photo-induced charge separation and light utilization ability. Up to now, two strategies were adopted to enhance the photocatalysis activity of UiO-66, including: (i) The introduction of conductors or semiconductors to UiO-66 to fabricate UiO-66-based composites (such as UiO-66/g-C_3N_4, NH_2-UiO-66/S–TiO_2, UiO-66/Ag_2CO_3) for enhanced Cr (VI) reduction (Li et al., 2020a; Yi et al., 2019a; Zhou et al., 2019); (ii) the introduction of functional groups such as amine (-NH_2) onto the organic ligands of UiO-66 to boost the photocatalytic performance, since the amine-functionalized UiO-66 (NH_2-UiO-66) displayed boarder visible light absorption, improved electron transportation from the organic linker to Zr–O clusters, and boosted excitation of Zr–O cluster. Our group fabricated NH_2-UiO-66(Zr) membrane to accomplish long-term (2400 min) operation for photocatalytic Cr(VI) elimination under white light (Du et al., 2019). Recently, $(OH)_2$-UiO-66 attracted increasing interest due to that the introduction of two –OH groups can achieve red-shifting of the light absorption edge, narrowing the energy gap, and enhancing the charge carrier separation (Xie et al., 2020; Wang et al., 2020).

Advanced reduction process (ARP) had been reported to remove oxidative pollutants in wastewater, in which the highly reductive chemicals might be involved (Milh et al., 2021). Carboxyl anion radicals ($COO\cdot^-$) represented a general reductive species for wastewater treatment. Despite relatively weak reducibility compared with electrons (Flyunt et al., 2001), $COO\cdot^-$ formed via a single electron transfer process between carboxylic acids with small molecule weight in photocatalysis, which can boost the Cr(VI) reduction (Perissinotti et al., 2001). Also, small organic acids (SOAs) were generally known as hole scavengers to accelerate the Cr(VI) reduction (Yang et al., 2010), in which SOAs could be oxidized by hydroxyl radicals (·OH) to produced $COO\cdot^-$ (Perissinotti et al., 2001). It was worth noting that Cr(VI) as appropriate electron scavenger can markedly promote the transfer electrons and the generated of $COO\cdot^-$ (Wang et al., 2009) Some SOAs including tartaric acid, citric acid and malic acid are easy to transfer electron via a charge-transfer-complex (CTC) - mediated pathway due to their special structure (Wang et al., 2010). Tartaric acid (TA), as a nature product, was used in various fields like silver mirrors, soft drinks, and tanning leather (Kaya et al., 2014). Therefore, it was feasible to use tartaric acid not only as electron transfer agent to yield $COO\cdot^-$ for enhancing the in-situ Cr(VI) reduction but also as hole scavenger to inhibit the recombination of photo-induced electron-hole pairs in a photocatalytic system.

This work developed a simple and mild synthesis method to fabricate the hydroxyl groups modified UiO-66 (i.e. $(OH)_2$-UiO-66-X%, X stands for the content ratio of input 2,5-dihydroxyterephthalic acid) via solvothermal reaction between zirconium tetrachloride and the mixture of benzene-1,4-dicarboxylic acid (H_2BDC) and 2,5-dihydroxyterephthalic acid (H_2BDC-$(OH)_2$) (Scheme 1). Hydroxyl groups were introduced as the intramolecular hole scavenger to promote the fast separation of photogenerated charge carrier (Wang et al., 2020). $(OH)_2$-UiO-66-X% could rapidly reduce Cr(VI) to Cr(III) under low power light illumination, in which the Box-Behnken design method was introduced to investigate the influence of co-existing inorganic ions on the reduction efficiency. The possible mechanisms of Cr(VI) reduction were proposed under the conditions with and without the presence TA.

2. Experimental

All chemicals were commercially available from J&K company, which were directly used without further treatment. All characterizations and tests were listed in electronic supplementary information (ESI).

2.1. Synthesis of $(OH)_2$-UiO-66-X%

The hydroxyl modified UiO-66 ($(OH)_2$-UiO-66-X%) was synthesized following the previously reported synthesis strategy of UiO-66 with modifications (Yi et al., 2019a). In brief, the solutions of 0.1716 mmol $ZrCl_4$ (40 mg) and 0.1716 mmol organic ligand dissolved respectively in 5.0 mL N,N-dimethylformamide (DMF) were mixed, in which the organic ligand was the matrix of benzene-1,4-dicarboxylic acid and 2, 5-dihydroxyterephthalic acid in different proportions. Then, 3.0 mL acetic acid was introduced to the mixed solution. The matrix was transferred into a 25.0 mL Teflon lined autoclave, followed by heating at 120 °C for 24 h. Finally, the $(OH)_2$-UiO-66-X% samples were obtained via centrifugation after cooling to ambient temperature, in which the "X" in $(OH)_2$-UiO-66-X% stands for the content ratio of input 2,5-dihydroxyterephthalic acid.

In this experiment, the proportions of the input 2,5-dihydroxyterephthalic acid in the organic ligand were 5%, 10%, 20%, and 40%, The obtained pale-yellow $(OH)_2$-UiO-66-X% powder samples were labeled as $(OH)_2$-UiO-66-5%, $(OH)_2$-UiO-66-10%, $(OH)_2$-UiO-66-20% and $(OH)_2$-UiO-66-40%, respectively.

2.2. Photocatalytic activity test

The photocatalytic Cr(VI) reduction tests of the $(OH)_2$-UiO-66-X% photocatalysts were carried out using $K_2Cr_2O_7$ as the model pollutant. 20.0 mg photocatalyst was suspended in 50.0 mL aqueous solution containing 10.0 mg L^{-1} $K_2Cr_2O_7$ as Cr(VI) model. The pH values of the solutions were adjusted by H_2SO_4 or NaOH solutions. The 10 W LED ultraviolet lamp (PCX50B, Beijing Perfect Light Technology Co., Ltd.) was selected as the light source to provide UV light with a 369 nm wavelength (the spectrum of the selected light source was displayed in Fig. S1). After adsorption-desorption equilibrium was accomplished, the system was exposed to UV light under magnetic stirring. Each 1.5 mL solution was extracted at specified time intervals and filtered using 0.45 μm PTFE membrane for further analysis. The residual Cr(VI) concentrations were determined using the diphenyl carbazide (DPC) approach

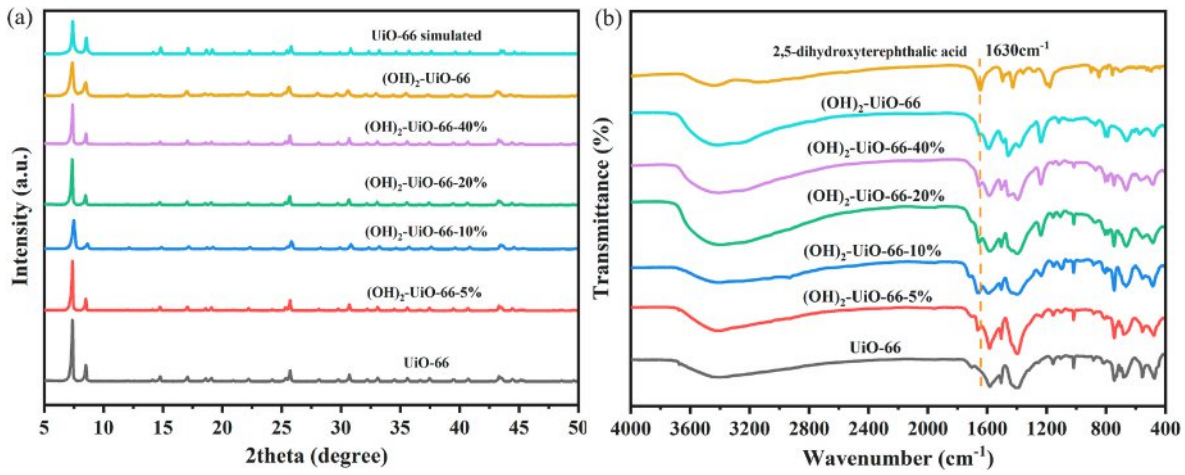

Fig. 1. (a) The PXRD patterns and (b) FTIR spectra of the UiO-66, series $(OH)_2$-UiO-66-X% and individual $(OH)_2$-UiO-66.

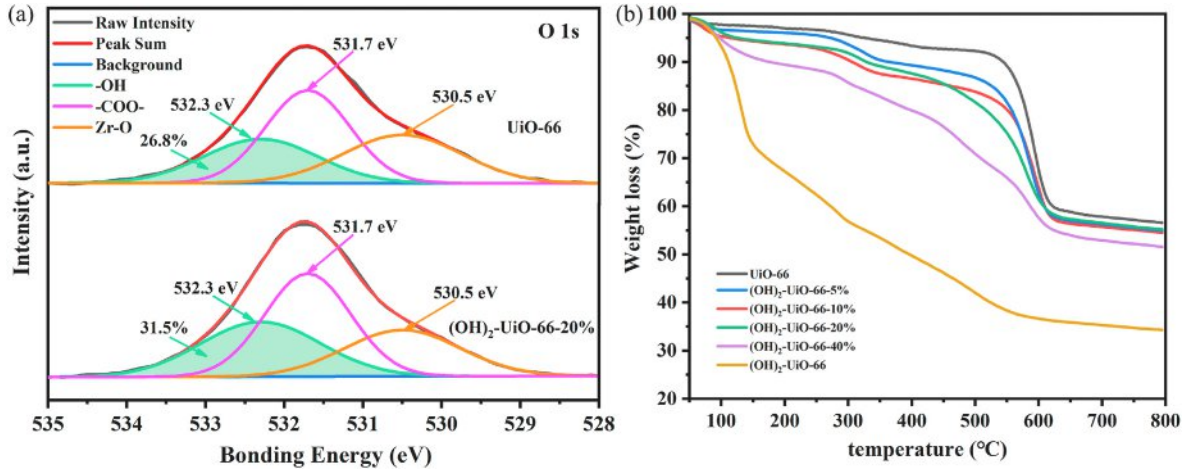

Fig. 2. (a) The spectra of O 1s of pristine UiO-66 and $(OH)_2$-UiO-66-20%. (b) TGA analyses of the UiO-66 and series $(OH)_2$-UiO-66-X%.

on Auto Analyzer 3 Flow Injection Analyzer (Chen et al., 2020).

The apparent quantum efficiency (AQE) experiments were performed upon the irradiation of different lights with selected wavelengths originated from 300 W Xe light (Beijing Aulight Co., Ltd) with the aid of different light filters. The AQEs of photocatalytic Cr(VI) reduction and the incident photons were calculated following Eqs. (1) and (2) (Velegraki et al., 2018; Li et al., 2019a).

$$AQE(Cr) = \frac{3 \times [number\ of\ reduced\ Cr(VI)]}{number\ of\ incident\ photons} \quad (1)$$

$$N_P^i = \frac{Pt\bar{\lambda}}{hc} \quad (2)$$

in which, P, t, and λ are the optical power, the irradiation time, and the light wavelength, respectively. h and c represent Planck constant of $6.62607015 \times 10^{-34}$ J s, and lightspeed of 299,792,458 m s^{-1}.

Table 1
Ratios of 1,4-dicarboxylic acid (H_2BDC) and 2,5-dihydroxyterephthalic acid (H_2BDC-$(OH)_2$) in $(OH)_2$-UiO-66-X% determined by TGA and element analysis.

NO.	Sample name	Input	EA and TGA
1	UiO-66	10:0	10:0
2	$(OH)_2$-UiO-66-5%	9.5:0.5	9.57:0.43
3	$(OH)_2$-UiO-66-10%	9:1	9.08:0.92
4	$(OH)_2$-UiO-66-20%	8:2	8.23:1.77
5	$(OH)_2$-UiO-66-40%	6:4	6.55:3.45
6	$(OH)_2$-UiO-66	0:10	0:10

3. Results and discussion

3.1. Characterizations

The powder X-ray diffraction (PXRD) patterns of pristine UiO-66, $(OH)_2$-UiO-66, and series $(OH)_2$-UiO-66-X% were depicted in Fig. 1a. The PXRD patterns of series $(OH)_2$-UiO-66-X% were very similar to that of UiO-66 (Yu et al., 2017; Ghorbanpour et al., 2018), with no other peaks observed, indicating that the original structures of $(OH)_2$-UiO-66 were well maintained. Fourier transform infrared spectra (FTIR) (Fig. 1b) was employed to check the modified hydroxyl groups on the surface of the as-prepared $(OH)_2$-UiO-66-X% surface. The peak around 1630 cm^{-1} could be attributed to the stretching vibration of hydroxyl groups in 2,5-dihydroxyterephthalic acid (Li et al., 2017).

X-ray photoelectron spectra (XPS) was adopted to further prove the amount of hydroxyl groups in $(OH)_2$-UiO-66-20%. The XPS survey scan (Fig. S2) of UiO-66 and $(OH)_2$-UiO-66-20% showed O 1s, C 1s, Zr 3d characteristic peaks. The O 1s signal (Fig. 2a) mainly demonstrated three peaks at 352.3 eV, 531.7 eV and 530.5 eV. The peaks at 531.7 eV and 530.5 eV were ascribed to –COO– group and Zr–O group, respectively (Shi et al., 2020; Lv et al., 2020). The primary peak at 532.3 eV can be assigned to the oxygen atom in the hydroxyl group (Bariki et al., 2020). Based on the peak area, which was proportional to the content of

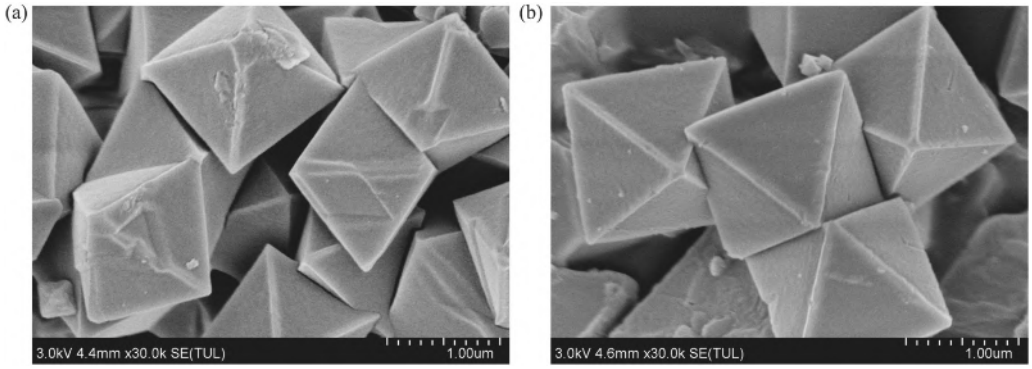

Fig. 3. The SEM images of (a) UiO-66 and (b) $(OH)_2$-UiO-66-20%.

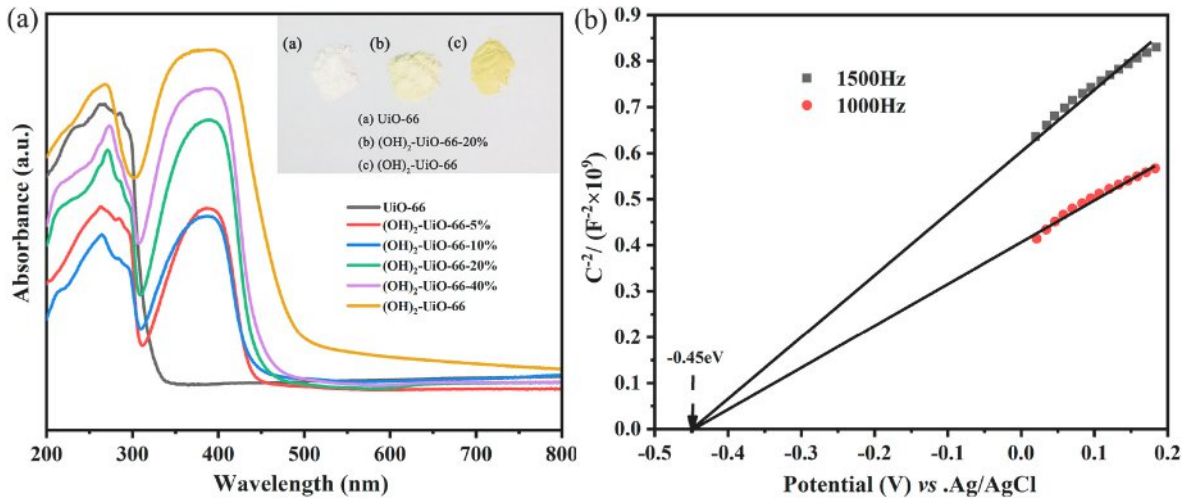

Fig. 4. (a) The UV–vis DRS of the UiO-66, series $(OH)_2$-UiO-66-X% and $(OH)_2$-UiO-66. Note: the inset pictures displayed the color of the UiO-66, $(OH)_2$-UiO-66-20% and $(OH)_2$-UiO-66 samples. (b) Mott-Schottky curves of $(OH)_2$-UiO-66-20% at different frequencies. (For interpretation of the references to color in this figure legend, the reader is referred to the Web version of this article.)

–OH (Li et al., 2017). The amount of hydroxyl groups on $(OH)_2$-UiO-66-20% were calculated as 31.5%, which was higher than 26.8% of UiO-66. From the above-stated XPS analysis, it can be concluded that 2,5-dihydroxyterephthalic acid was coordinated with zirconium in the UiO-66 structure.

The introduced H_2BDC-$(OH)_2$ contents in $(OH)_2$-UiO-66-X% were further determined by both thermogravimetric analyses (TGA) (Fig. 2b) and CHO elemental analyses (EA). The input ratios and the calculated ratios of H_2BDC and H_2BDC-$(OH)_2$ in the different $(OH)_2$-UiO-66-X% (Table 1) were calculated from Eqs. S1 and S2. It was observed that the actual contents (the calculated ratios) of two ligands into $(OH)_2$-UiO-66-X% matched well with the input ratios. For example, the input ratio and the calculated ratio of H_2BDC and H_2BDC-$(OH)_2$ in $(OH)_2$-UiO-66-20% were 8.0:2.0 and 8.23:1.77, respectively.

The scanning electron microscope (SEM) images revealed that both pristine UiO-66 and $(OH)_2$-UiO-66-20% displayed smooth octahedral morphology with particle size in the range of 1300–1500 nm (Fig. 3a and b). However, the individual $(OH)_2$-UiO-66 (Fig. S3) displayed irregular-shaped particles with sizes ranging from 80 to 200 nm, which was comparable to that of previous report (Xie et al., 2020).

The UV–Vis diffuse reflectance spectra (UV–vis DRS) showed the absorption properties of series $(OH)_2$-UiO-66-X%. As demonstrated in Fig. 4a, the series $(OH)_2$-UiO-66-X% could be excited by both ultraviolet light and visible light. Comparing with the pristine UiO-66, the red shift of $(OH)_2$-UiO-66-X% can be ascribed to that the introduced hydroxyl group could improve the light absorption for longer wavelength (Xie et al., 2020). The color of UiO-66, $(OH)_2$-UiO-66-20% and $(OH)_2$-UiO-66 powder were white and pale-yellow, respectively (inset pictures in Fig. 4a).

The Mott-Schottky plots of the $(OH)_2$-UiO-66-20% were determined at different frequencies to calculate the flat band potential (Fig. 4b). The positive relationship and the obtained C^{-2} to the potentials implied that the corresponding photocatalysts belonged to n-type semiconductors (Shen et al., 2015). The conduction band (LUMO) of the $(OH)_2$-UiO-66-20% was determined to be ca. −0.45 eV *versus* the Ag/AgCl electrode at pH = 7.0 via $E_{LUMO} = E_{HOMO} - E_g$ (Zou et al., 2016). Since the flat band potential is more positive 0.1 eV than the conduction band potential for n-typed semiconductor (Zhao et al., 2020), the E_{LUMO} of $(OH)_2$-UiO-66-20% was calculated as −0.35 eV *vs*. NHE. Considering the pH effect, the following Eq. (3) (Liu et al., 2020b) was used to correct the E_{LUMO} and E_{HOMO} of $(OH)_2$-UiO-66-20%.

$$E = E_0 - 0.05915 \times \text{pH} \quad (3)$$

The E_{LUMO} and E_{HOMO} values of $(OH)_2$-UiO-66-20% at pH = 7.0 were estimated to be −0.76 and 3.22 eV *vs*. NHE.

3.2. Photocatalytic performances

3.2.1. Photocatalytic Cr(VI) reduction performances of $(OH)_2$-UiO-66-X%

The Cr(VI) reduction experiments were performed under the low power LED UV light irradiation. The adsorption capacities of $(OH)_2$-UiO-66-X% increased with the increasing hydroxyl group content due to the

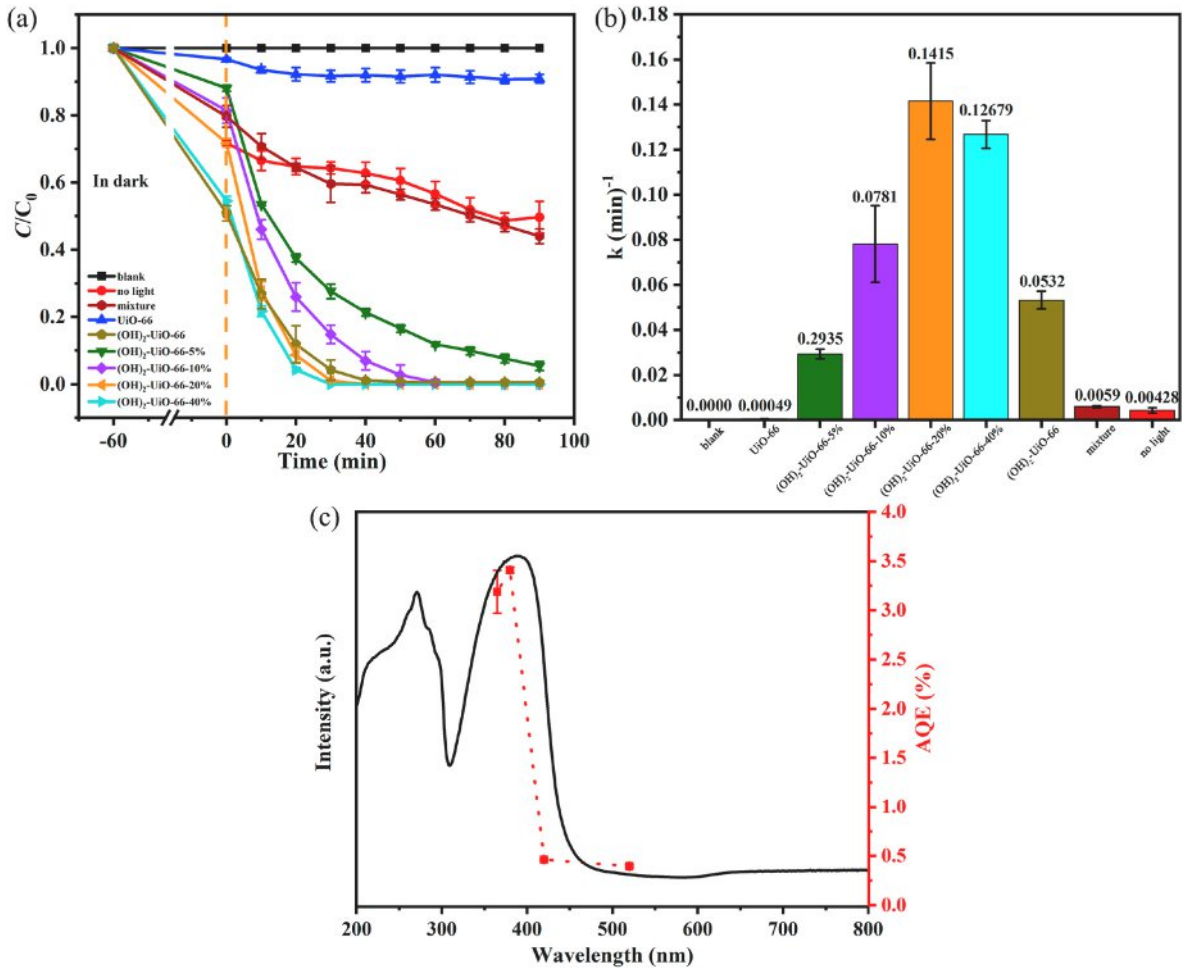

Fig. 5. The photocatalytic Cr(VI) reduction (a) efficiencies and (b) rates (*k* values) over the photocatalysts under LED UV light irradiation. (c) AQEs of Cr(VI) reduction upon the irradiation of different lights.

enough electrostatic interaction sites for adsorbing Cr(VI) ions (Fig. 5a) (Li et al., 2017; Nair et al., 2014), which further resulted in the better photocatalytic Cr(VI) reductions performances of all $(OH)_2$-UiO-66-X% than that of the pristine UiO-66. In detail, $(OH)_2$-UiO-66-20% showed the highest photocatalytic Cr(VI) reduction efficiency (98.97% at 30 min, 100% within 40 min), and followed by $(OH)_2$-UiO-66-5% (72.40% at 30 min, 94.57% within 90 min), $(OH)_2$-UiO-66-10% (85.20% at 30 min, 100% within 70 min). In addition, the $(OH)_2$-UiO-66-20% photocatalyst exhibited superior photocatalytic Cr(VI) reduction activity to many counterparts photocatalysts (Table 2). The Cr(VI) removal efficiency of $(OH)_2$-UiO-66-40% reached 100% in 30 min, which was comparable to that of $(OH)_2$-UiO-66-20%. However, the high removal efficiency of $(OH)_2$-UiO-66-40% can be ascribed to both adsorption (45.52%) and photocatalysis (54.48%) procedures, in which excessive adsorption of Cr(VI) onto photocatalyst might result in the mask of active sites and the poor reusability (Li et al., 2020a). Besides, the pseudo-first-order kinetic (*k*) model (Eq. (4)) was adopted to quantitatively describe the reaction kinetics. The photocatalysis reaction rate evidenced by reaction rate constant *k* (Fig. 5b) followed the order of $(OH)_2$-UiO-66-20% > $(OH)_2$-UiO-66-40% > $(OH)_2$-UiO-66-10% > $(OH)_2$-UiO-66 > $(OH)_2$-UiO-66-5% > mixture > no light > UiO-66. From these results, the net photocatalysis efficiency of $(OH)_2$-UiO-66-40% was lower than that of $(OH)_2$-UiO-66-20%. Therefore, $(OH)_2$-UiO-66-20% was selected as optimal photocatalyst to complete the further experiments and determinations.

$$\ln(C / C_0) = -kt \quad (4)$$

As shown in Fig. S4 and Table S1, the results of the Brunauer-Emmett-Teller (BET) specific surface area indicated that the partial introduction of 2,5-dihydroxyterephthalic acid did not led to the big

Table 2
Comparisons of the photocatalytic Cr(VI) reduction activities of some selected counterpart photocatalysts.

Photocatalyst/amount (mg)	C_0 (mg L^{-1})	Light source	*T* (min)	1st cycle efficiency (%)	Ref.
UiO-66-NH_2 membrane	5.0	300 W Xe lamp	120	98	Du et al. (2019)
3.0-HUCN/100	20.0	300 W Xe lamp	60	100	Wang et al. (2020)
UiO-66-NH_2/20	10.	300 W Xe lamp	80	97	Shen et al. (2015)
g-C_3N_4/MIL-100(Fe)/100	10.0	300 W Xe lamp	80	97	Yi et al. (2019b)
WO_3/MIL-100 (Fe)/20	5.0	25 W LED lamp	60	100	Wang et al. (2021b)
Ag_2CO_3/UiO-66-NH_2/10	10.0	5 W LED lamp	50	100	Zhou et al. (2019)
S–TiO_2/UiO-66-NH_2/10	5.0	300 W Xe lamp	75	100	Li et al. (2020a)
$(OH)_2$-UiO-66-20%/20	10.0	10 W LED lamp	40	100	This work

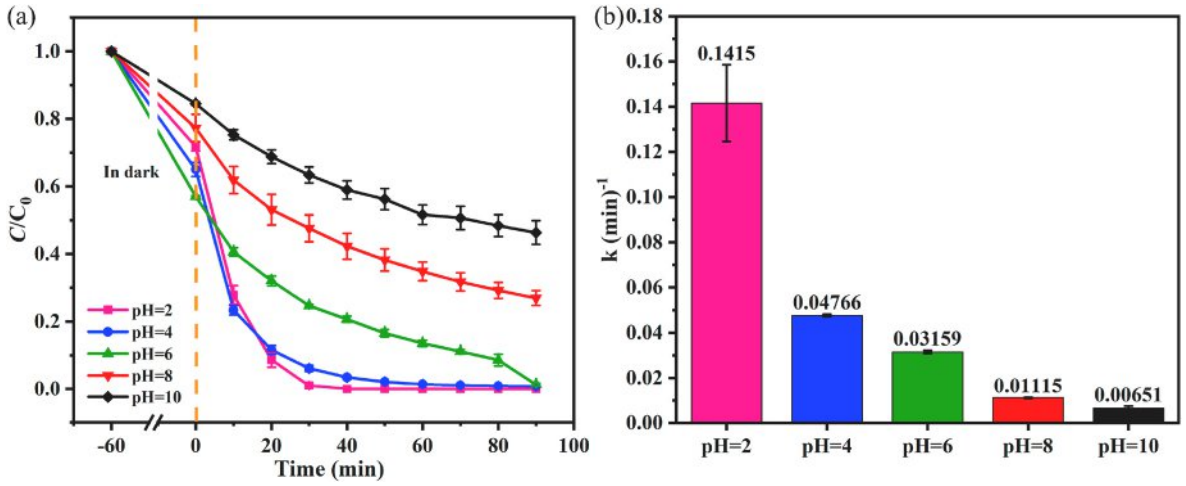

Fig. 6. The influences of initial pH values on (a) the Cr(VI) reduction efficiencies and (b) rates (*k* values).

surface areas decrease of $(OH)_2$-UiO-66-X%. However, as the proportion of 2,5-dihydroxyterephthalic acid increased to 40%, the specific surface area decreased from 1079.2 $m^2\ g^{-1}$ to 922.46 $m^2\ g^{-1}$. The larger specific surface areas were believed to expose more active sites, which can improve the photocatalysis activities via improving the charge transfer and effective light utilization (Chen et al., 2007).

The AQE determination was selected as a critical index to evaluate photocatalysis abilities under different light sources (Li et al., 2019b). As illustrated in Fig. 5c, the AQEs of $(OH)_2$-UiO-66-20% achieved 3.13%, 3.37%, 0.24% and 0.17% upon the irradiation of different lights with wavelengths at 365 nm, 380 nm, 420 nm and 520 nm, respectively. The AQEs at different wavelengths followed the curve trend of the used UV–vis DRS spectra, confirming that the Cr(VI) reduction over $(OH)_2$-UiO-66-20% was subject to the photocatalysis procedure (Zhou et al., 2020; Wang et al., 2021a).

3.2.2. *Effect of initial pH toward Cr(VI) reduction*

It was thought that pH might exert significant influence to the Cr(VI) reduction (Wang et al., 2016a), since it can change both the Zeta potentials of the selected photocatalysts and the existing forms of Cr(VI) (Yi et al., 2019b). In this study, the Cr(VI) reduction experiments were performed at pH = 2.0, 4.0, 6.0, 8.0, 10.0, respectively. It had been reported that the pH values of solutions could influence the surface potential of the photocatalyst (Grover et al., 2013). As shown in Fig. S5, the zeta potentials of $(OH)_2$-UiO-66-20% were positive at pH = 2.0, 4.0 and 6.0, which facilitated the Cr(VI) adsorption under acid conditions due to the electrostatic attraction. In contrast, its zeta potentials were negative at pH = 8.0 and 10.0, which restrained the Cr(VI) adsorption because of strong electrostatic repulsion. As illustrated in Fig. 6a and b, it was also observed that pH exerted heavily influences toward both the Cr(VI) reduction efficiencies and rates (*k* values), in which higher pH led to decline efficiency and reaction rate. The processes of photocatalytic Cr(VI) reduction over $(OH)_2$-UiO-66-X% followed by Eqs. (5) and (6) under acidic solution (Du et al., 2019; Wang et al., 2017). The abundant H^+ ions in solution were conducive to the Cr(VI) transformation to Cr (III) (Wang et al., 2016a). In contrast, the Cr(VI) existence form was CrO_4^{2-} under higher pH environment (Zhang et al., 2017), in which the Cr(VI) reduction reaction was achieved following Eq. (7) (Yi et al., 2019b). As well, the formed solid $Cr(OH)_3$ under higher pH conditions might mask the active sites of $(OH)_2$-UiO-66-20% photocatalyst, resulting in the decreased Cr(VI) reduction performance (Wang et al., 2015, 2016a).

$$(OH)_2 - UiO - 66 - 20\% + h\nu \rightarrow (OH)_2 - UiO - 66 - 20\% (h^+ + e^-) \quad (5)$$

$$Cr_2O_7^{2-} + 14H^+ + 6e^- \rightarrow 2Cr^{3+} + 7H_2O \quad (6)$$

$$CrO_4^{2-} + 4H_2O + 3e^- \rightarrow Cr(OH)_3 + 5OH^- \quad (7)$$

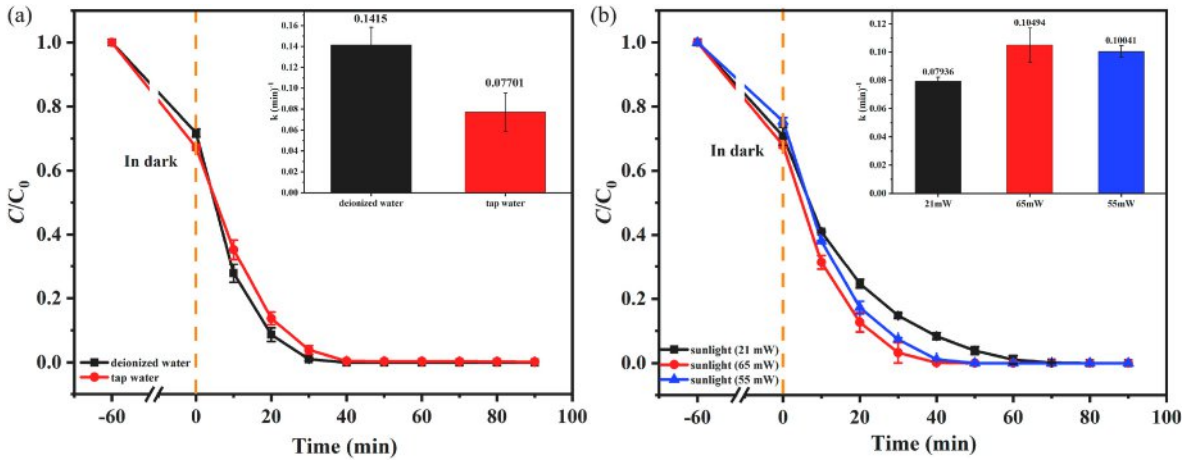

Fig. 7. The Cr(VI) reduction efficiencies and the corresponding reduction rates (*k* values) (inset plots) over $(OH)_2$-UiO-66-20% (a) in different wastewater samples simulated from both deionized water and tap water, as well as (b) under sunlight irradiation.

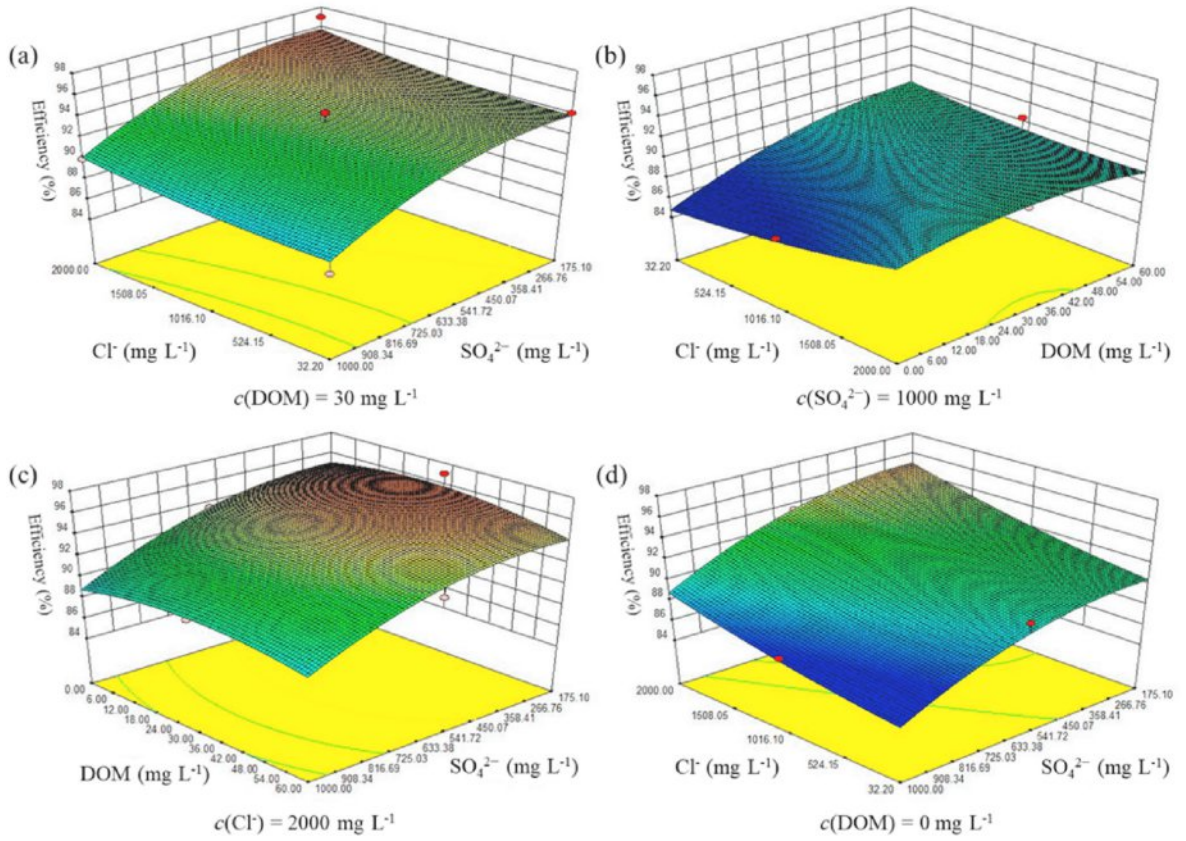

Fig. 8. Response surface diagram of the influences from different co-existing matters in simulation tanning wastewater toward Cr(VI) reduction efficiencies over $(OH)_2$-UiO-66-20%.

3.2.3. *Photocatalytic Cr(VI) reduction performance in the simulated tannery wastewater*

Different simulated wastewater containing Cr(VI) formulated by tap water and deionized water (the quality parameters of corresponding water sample was shown in Table S2) were tested for $(OH)_2$-UiO-66-20% under UV light irradiation. As shown in Fig. 7a, the Cr(VI) reduction performances over $(OH)_2$-UiO-66-20% decreased slightly in simulated Cr(VI) wastewater from tap water, in which 100% Cr(VI) can be accomplished within 60.0 min.

Considering that $(OH)_2$-UiO-66-20% could be excited by the visible light (Fig. 4a), In this study, the experiments were performed under real solar at the Daxing campus of BUCEA (39°44′ N, 116°17′ E) on February 9th (15 °C), March 16th (14 °C) and March 21st (12 °C) in 2021. The optical powers were measured as 21 mW, 65 mW and 55 mW the spectrum of real sunlight were shown in Fig. S6. As illustrated in Fig. 7b, the 100% Cr(VI) reduction can be accomplished within 70 min, 40 min and 50 min on February 9th, March 16th and March 21st, respectively. Therefore, the real sunlight can induce the photocatalysis reaction by $(OH)_2$-UiO-66-20%, in which the optical power was thought as one of the primary factors for effective Cr(VI) reduction via photocatalysis.

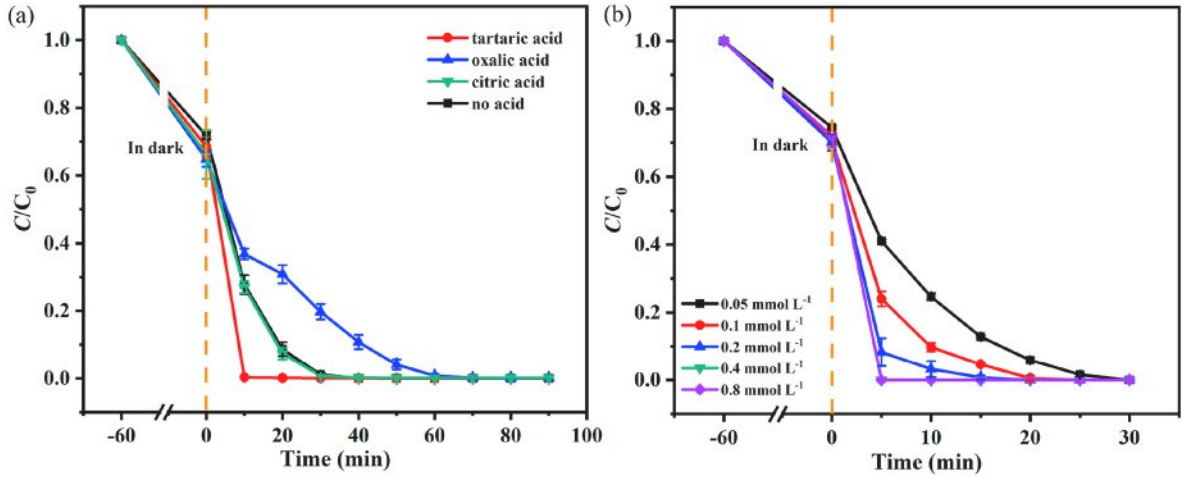

Fig. 9. The influences of (a) different small molecule acids and (b) the tartaric acid concentrations on photocatalytic Cr(VI) reduction performances over $(OH)_2$-UiO-66-20% photocatalyst.

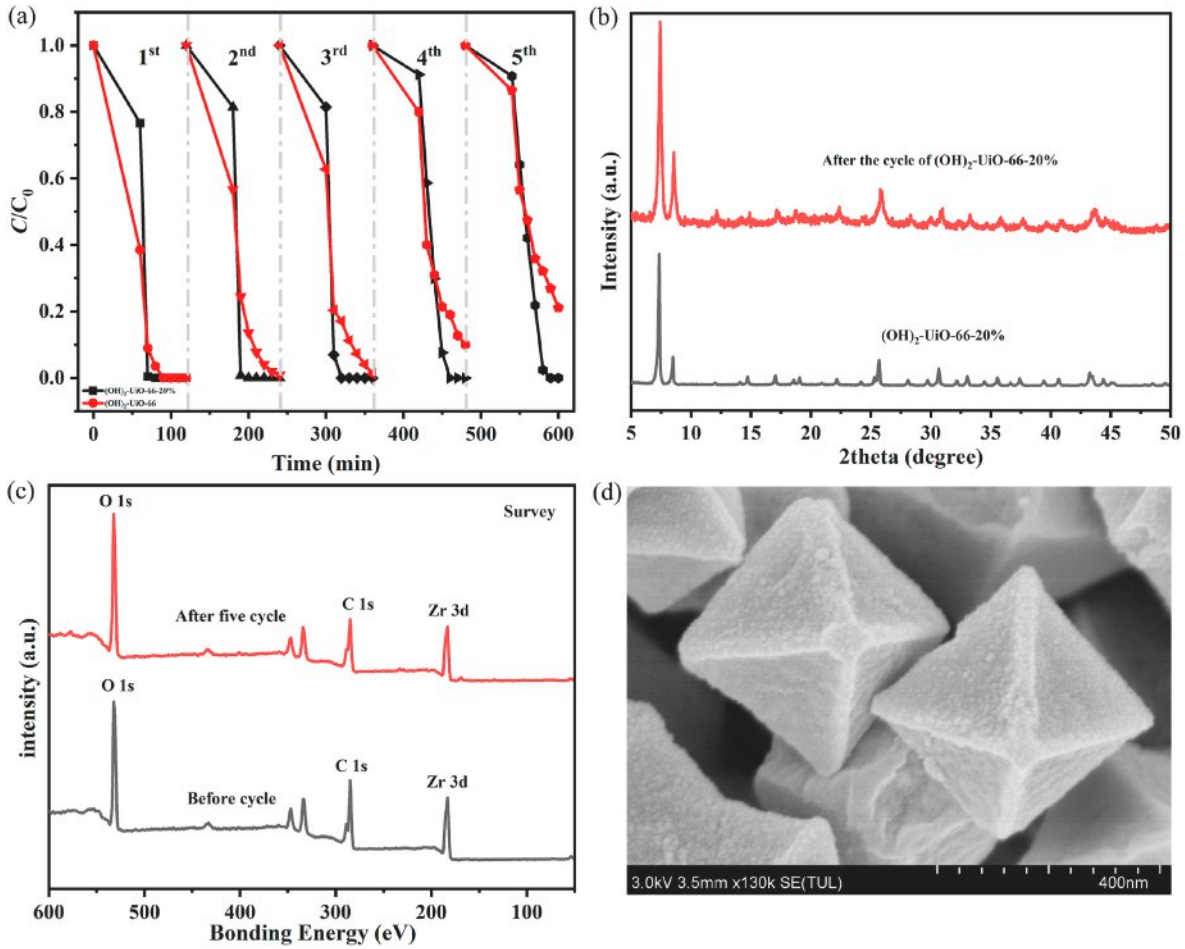

Fig. 10. (a) The cyclic performance of Cr(VI) removal over $(OH)_2$-UiO-66-20% and $(OH)_2$-UiO-66. (b) PXRD patterns (c) XPS survey spectra of $(OH)_2$-UiO-66-20% before and after recyclability. (d) the SEM image of $(OH)_2$-UiO-66-20% after the photocatalytic activities. Reaction conditions: 0.4 mg L^{-1} photocatalyst, 10 mg L^{-1} Cr(VI) and 0.2 mmol L^{-1} tartaric acid.

The effect of co-existing inorganic ions in tanning wastewater was also studied by the Box-Behnken methodology (Li et al., 2020a; Zhao et al., 2020). It was believed that the photo-generated electrons or holes are free of the influence of the inorganic cations like K^+, Ca^{2+}, Na^+, Mg^{2+} because of the high stability of these cations (Yi et al., 2019a; Wang et al., 2012). Abundant SO_4^{2-} (175.1–1000 mg L^{-1}) and Cl^- (32.2–2000 mg L^{-1}) existed in tanning wastewater might exerted great influence to the photocatalysis activity. Therefore, the effect of the co-existed SO_4^{2-} (A), Cl^- (B) and DOM (C, tartaric acid as DOM model) was tested to explore the photocatalytic Cr(VI) reduction efficiencies under LED UV light irradiation, in which the ion concentrations of natural lake water was lowest and that of tanning wastewater was highest. The 17 runs experiments results (Table S3) indicated that the quadratic polynomial model (Eq. (8)) could be used to describe the relationship between the photocatalytic efficiency response and variables.

$$\text{Efficiency}\% = 93.36 + 0.82\,A - 2.69\,B + 1.20\,C - 0.13\,AB - 1.32\,AC + 0.30\,BC + 0.45\,A^2 - 1.63\,B^2 - 1.17\,C^2 \quad (8)$$

The calculated F values were 41.33, 8.23, 3.80 for SO_4^{2-}, DOM and Cl^-, respectively, demonstrating that SO_4^{2-} and DOM rather than Cl^- can exert obvious impact on Cr(VI) reduction. As depicted in the 3D surface plots (Fig. 8), the selected inorganic anions especially SO_4^{2-} could inhibit the Cr(VI) reduction (Fig. 8d), in which $(OH)_2$-UiO-66-20% could adsorb SO_4^{2-} via the electronic interactions (Yi et al., 2019a). As to the simulated wastewater containing SO_4^{2-} (1000 mg L^{-1}) and Cl^- (2000 mg L^{-1}), the influence of TA concentration toward Cr(VI) reduction displayed saddle-shaped curve (Fig. 8b and c), in which the optimal concentration of tartaric acid was 0.2 mmol L^{-1}.

3.2.4. *Influence of small molecular organic acids*

The results of Box-Behnken experiment revealed that the Cr(VI) reduction activity over $(OH)_2$-UiO-66-20% was further boosted when tartaric acid was introduced. Three small molecular organic acids (SOAs) including citric acid, oxalic acid and tartaric acid were introduced into the aqueous solution to explore their influences on the photocatalytic Cr(VI) reduction performance of $(OH)_2$-UiO-66-20% (Fig. 9a). Generally, SOAs were adopted as hole scavengers in the photocatalytic reaction, which consumed the photo-induced holes (h^+) to accelerate the Cr(VI) reduction via enhancing the separation of photo-induced electron-hole pairs (Yi et al., 2019a; Wang et al., 2021b). However, among the three SOAs in our study, only tartaric acid could accelerate the Cr(VI) reduction in the photocatalysis reaction (Fig. 9a), which could be attributed to the different structures of SOAs (Wang et al., 2008, 2016a). The Cr(VI) reduction efficiency declined when ·OH had been trapped by oxalic acid (Liu et al., 2021), which could shift the equilibrium toward Cr(VI) as indicated in Eqs (9)–(11) (Yi et al., 2019a). The consumed ·OH would also hinder the separation of electrons and holes to further decrease the Cr(VI) reduction efficiency. However, the increased photocatalytic Cr(VI) reduction rate under UV light irradiation was originated from the electron transfer between tartaric acid and $(OH)_2$-UiO-66-20%. Tartaric acid could coordinate with photocatalyst $(OH)_2$-UiO-66-20% to form charge-transfer-complex (CTC), which leads to the migration of the photo-produced electrons from tartaric acid to

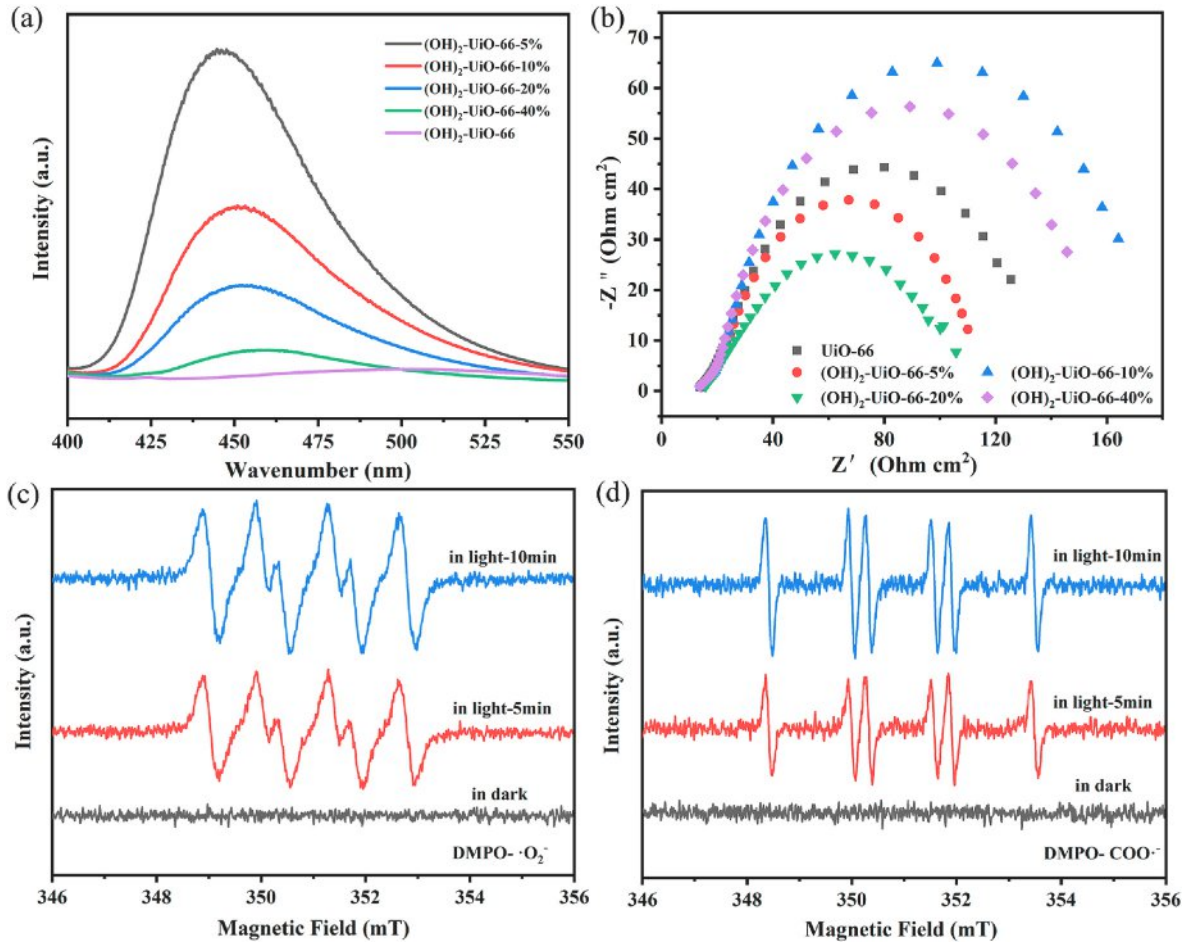

Fig. 11. The (a) PL spectra, (b) EIS analysis of different photocatalysts. The ESR spectra of active species trapped by DMPO over $(OH)_2$-UiO-66-20% in aqueous solution for (c) $\cdot O_2^-$ and (d) $COO\cdot^-$.

the LUMO of the $(OH)_2$-UiO-66-20% (Wang et al., 2010). During this process, $COO\cdot^-$ radicals were produced from tartaric acid to participate and enhance the Cr(VI) reduction (Wang et al., 2010; Zhao et al., 2021). To explore the follow-up work, the photocatalytic Cr(VI) reduction performances of all photocatalysts were improved significantly after 0.1 mmol L^{-1} TA was added (Fig. S7). It was worth mentioning that the TA could only reduce partial Cr(VI) under UV light irradiation. The rate diagram indicated that $(OH)_2$-UiO-66-20% was the most effective photocatalyst with highest reaction rates (k values) of 0.2234 min^{-1} (Fig. S8).

The concentration of TA could also affect the reduction process due to the release of free radicals (Liu et al., 2021). As depicted in Fig. 9b, the Cr(VI) reduction efficiencies increased as the tartaric acid concentrations increased from 0.05 to 0.4 mmol L^{-1}. However, the reduction efficiencies did not change significantly when the TA concentration was increased to 0.8 mmol L^{-1}, indicating that excessive tartaric acid would neither consume the photo-induced free radicals nor produce more $COO\cdot^-$ radicals. The reaction involved $COO\cdot^-$ radicals might be expressed by Eq. (12) (Liu et al., 2021).

$$O_2 + e^- \rightarrow \cdot O_2^- \quad (9)$$

$$2\cdot O_2^- + 2H^+ \rightarrow H_2O_2 + O_2 \quad (10)$$

$$H_2O_2 + Cr(III) + H^+ \rightarrow Cr(VI) + H_2O + \cdot OH \quad (11)$$

$$Cr_2O_7^{2-} + 6COO\cdot^- + 14H^+ \rightarrow 2Cr^{3+} + 6CO_2 + 7H_2O \quad (12)$$

3.2.5. *Cyclicity and stability of $(OH)_2$-UiO-66-20%*

To explore the practical application of $(OH)_2$-UiO-66-20% photocatalyst in the treatment of industrial wastewater with optimal concentration of tartaric acid, five runs' Cr(VI) reduction operations were conducted with the presence of tartaric acid (0.2 mmol L^{-1}). As depicted in Fig. 10a, nearly 100% Cr(VI) reduction efficiencies can be accomplished over $(OH)_2$-UiO-66-20% photocatalyst after 5th run' operations, implying that $(OH)_2$-UiO-66-20% photocatalyst was stable and could be adopted for long-term operation. Meanwhile, the stability of $(OH)_2$-UiO-66-20% was further confirmed by PXRD (Fig. 10b), SEM (Fig. 10d), FITR (Fig. S9) and XPS (Fig. S10) analysis. Noticeably, the peaks at 580.2 eV and 586.8 eV could be assigned to Cr(VI), and the peak at 577.2 eV could be ascribed to the newly formed Cr(III) (Zhao et al., 2014; Libenson and Shakhmin, 2000), implying that both minor unreacted Cr(VI) and formed Cr(III) were adsorbed onto $(OH)_2$-UiO-66-20%.

3.3. *The photocatalytic Cr(VI) reduction mechanism*

Both photoluminescence (PL) spectroscopy and electrochemical impedance spectroscopy (EIS) were used to investigate the Cr(VI) reduction mechanism over $(OH)_2$-UiO-66-X% photocatalyst with or without the presence tartaric acid. The higher photoluminescence intensity indicated the higher recombination efficiency of photoinduced electrons and holes (Nie et al., 2018; Li et al., 2020b). As shown in Fig. 11a, it was clearly observed that the emission peak at 369 nm decreased with the increasing content of hydroxyl groups into $(OH)_2$-UiO-66-X%. It was deemed that the introduced hydroxyl groups in $(OH)_2$-UiO-66-X% could accomplish effective separation of the

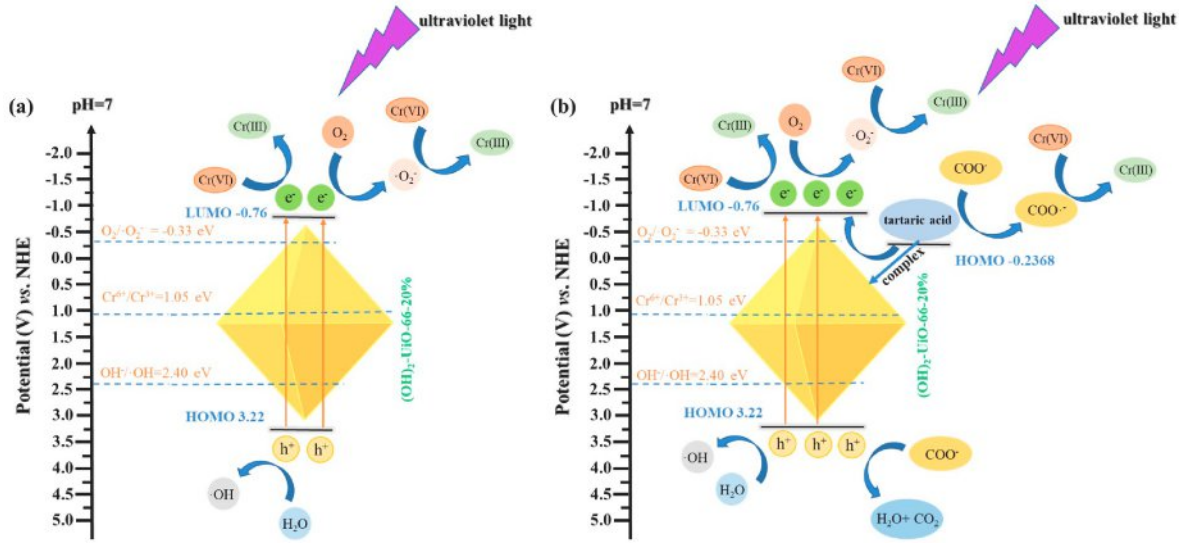

Fig. 12. The possible mechanisms of photocatalytic Cr(VI) reduction over $(OH)_2$-UiO-66-20% (a) without tartaric acid and (b) with tartaric acid.

electron - hole pairs (Ding et al., 2020). Although the $(OH)_2$-UiO-66-40% and $(OH)_2$-UiO-66 exhibited the more rapid charge carrier separation and migration rate, the decrease of their specific surface areas (Table S1) might lead to less exposure of active sites. The diameter of arc radius (Fig. 11b) of EIS determination results followed the order of $(OH)_2$-UiO-66-10% > $(OH)_2$-UiO-66-40% > UiO-66 > $(OH)_2$-UiO-66-5% > $(OH)_2$-UiO-66-20%, confirming that $(OH)_2$-UiO-66-20% displayed quicker charge carrier separation and interfacial charge transfer than other $(OH)_2$-UiO-66-X% photocatalysts.

To further identify the primary active species during the Cr(VI) reduction process and the corresponding reaction mechanism with or without tartaric acid, the ESR measurements were conducted. It was reported that $\cdot O_2^-$ radicals can participate the Cr(VI) reduction (Eqs. (13) and (14)) (Li et al., 2019a; Zhang et al., 2018b; Wang et al., 2016b).

$$\cdot O_2^- + Cr(VI) \rightarrow Cr(V) + O_2 \quad (13)$$

$$Cr(V) + 2e^- \rightarrow Cr(III) \quad (14)$$

In our work, the DMPO-$\cdot O_2^-$ signals (Fig. 11c) were observed upon the irradiation of UV light for 5 min and 10 min, affirming that $\cdot O_2^-$ radicals were produced in the photocatalysis process in the absence of tartaric acid. Based on the obtained results, the Cr(VI) reduction over $(OH)_2$-UiO-66-20% was proposed as illustrated in Fig. 12a. Both the photo-induced elections by $(OH)_2$-UiO-66-20% can not only directly reduce Cr(VI) to Cr(III) but also react with dissolved oxygen (DO) to produce $\cdot O_2^-$ radicals for Cr(VI) reduction. The photo-induced h^+ can react with water molecules to form ·OH radicals, which might oxide negligible Cr(III) to Cr(VI) (Yi et al., 2019a).

As shown in Fig. 12b, in addition to the participation of photo-induced electrons and $\cdot O_2^-$ radicals, the added tartaric acid (TA) can enhance Cr(VI) reduction via three channels: (i) TA acts as holes capturer to consume the holes to accelerate the charge carrier separation (Wang et al., 2021b); (ii) TA reacted with $(OH)_2$-UiO-66-20% to form charge-transfer-complex (CTC), which leaded to photo-produced electrons transfer from the HOMO of tartaric acid to the LUMO of the $(OH)_2$-UiO-66-20% (Wang et al., 2010); (iii) $COO\cdot^-$ radicals can be yielded from tartaric acid to enhance the Cr(VI) reduction. The $^-$·OOC-DMPO· signals (Fig. 11d) in the presence of TA were detected in ESR determination under UV light irradiation for 5 min and 10 min, confirming that $COO\cdot^-$ radicals could be yielded in the photocatalysis process using $(OH)_2$-UiO-66-20%.

4. Conclusion

Hydroxyl-modified UiO-66 was fabricated via the hydrothermal approach, in which the hydroxyl groups acted as the intermolecular hole scavenger to enhance the rapid separation of the photogenerated charge carrier. Under low-power LED UV light irradiation, $(OH)_2$-UiO-66-20% exhibited higher efficiency than UiO-66 and $(OH)_2$-UiO-66 for photocatalytic Cr(VI) reduction. The influences of SOAs, pH and co-existing matters on Cr(VI) reduction performances of $(OH)_2$-UiO-66-20% were explored. The Box-Behnken design approach was introduced to further declare that the inorganic foreign anions and dissolved organic matters (SOAs) could lead to significant impact on Cr(VI) reduction performance, which was promising for the application of Cr(VI) removal in tanning wastewater. The introduction of hydroxyl groups can extend the light absorption region longer wavelength even to shift to visible light, which provided possibility to use real sunlight to drive the Cr(VI) reduction. The recycling experiment showed that $(OH)_2$-UiO-66-20% had great reusability and stability for potential applications. This work provided a brand-new possibility to design and produce novel photocatalysis systems by surface modified MOF-based photocatalysts as well as the introduction of effective SOAs for enhanced Cr(VI) elimination for practical applications.

Declaration of competing interest

The authors declare that they have no known competing financial interests or personal relationships that could have appeared to influence the work reported in this paper.

Acknowledgements

This work was supported by National Natural Science Foundation of China (51878023), Beijing Natural Science Foundation (8202016), Great Wall Scholars Training Program Project of Beijing Municipality Universities (CIT&TCD20180323), Beijing Talent Project (2020A27) and The Fundamental Research Funds for Beijing University of Civil Engineering and Architecture (X20147/X20141/X20135/X20146).

Appendix A. Supplementary data

Supplementary data to this article can be found online at https://doi.org/10.1016/j.envres.2021.111596.

Credit author statement

Yu-Hang Li: Data curation, Investigation, Visualization, Writing – original draft preparation. Xiao-Hong Yi: Investigation, Methodology. Yu-Xuan Li: Software, Methodology. Chong-Chen Wang: Conceptualization, Funding acquisition, Supervision, Project administration, Writing – review & editing. Peng Wang: Resources, Instrumental. Chen Zhao: Review, Software. Weiwei Zheng: Supervision, Writing – review & editing.

References

Bariki, R., Majhi, D., Das, K., Behera, A., Mishra, B.G., 2020. Facile synthesis and photocatalytic efficacy of UiO-66/$CdIn_2S_4$ nanocomposites with flowerlike 3D-microspheres towards aqueous phase decontamination of triclosan and H_2 evolution. Appl. Catal. B Environ. 270, 118882.

Cavka, J.H., Jakobsen, S., Olsbye, U., Guillou, N., Lamberti, C., Bordiga, S., Lillerud, K.P., 2008. A new zirconium inorganic building brick forming metal organic frameworks with exceptional stability. J. Am. Chem. Soc. 130 (42), 13850–13851.

Chen, X., Yu, T., Fan, X., Zhang, H., Li, Z., Ye, J., Zou, Z., 2007. Enhanced activity of mesoporous Nb_2O_5 for photocatalytic hydrogen production. Appl. Surf. Sci. 253 (20), 8500–8506.

Chen, G., Han, J., Mu, Y., Yu, H., Qin, L., 2019. Two-stage chromium isotope fractionation during microbial Cr(VI) reduction. Water Res. 148, 10–18.

Chen, D.-D., Yi, X.-H., Zhao, C., Fu, H., Wang, P., Wang, C.-C., 2020. Polyaniline modified MIL-100(Fe) for enhanced photocatalytic Cr(VI) reduction and tetracycline degradation under white light. Chemosphere 245, 125659.

Ding, J.-F., Lu, S.-H., Shen, L., Yan, R.-P., Zhang, Y.-N., Zhang, H.-J., 2020. Enhanced photocatalytic reduction for the dechlorination of 2-chlorodibenzo-p-dioxin by high-performance g-C_3N_4/NiO heterojunction composites under ultraviolet-visible light illumination. J. Hazard Mater. 384, 121255.

Du, X.-D., Yi, X.-H., Wang, P., Zheng, W., Deng, J., Wang, C.-C., 2019. Robust photocatalytic reduction of Cr(VI) on UiO-66-NH_2(Zr/Hf) metal-organic framework membrane under sunlight irradiation. Chem. Eng. J. 356, 393–399.

Du, J., Zhang, B., Li, J., Lai, B., 2020. Decontamination of heavy metal complexes by advanced oxidation processes: a review. Chin. Chem. Lett. 31 (10), 2575–2582.

Flyunt, R., Schuchmann, M.N., von Sonntag, C., 2001. A common carbanion intermediate in the recombination and proton-catalysed disproportionation of the carboxyl radical anion, $\cdot CO_2^-$, in aqueous solution. Chemistry 7 (4), 796–799.

Fu-Xue, W., Chong-Chen, W., Peng, W., Bi-Cong, X., 2017. Syntheses and applications of UiO series of MOFs. Chin. J. Inorg. Chem. 33 (5), 713–737.

Ghorbanpour, A., Huelsenbeck, L.D., Smilgies, D.-M., Giri, G., 2018. Oriented UiO-66 thin films through solution shearing. CrystEngComm 20 (3), 294–300.

Grover, I.S., Singh, S., Pal, B., 2013. The preparation, surface structure, zeta potential, surface charge density and photocatalytic activity of TiO_2 nanostructures of different shapes. Appl. Surf. Sci. 280, 366–372.

Heidmann, I., Calmano, W., 2008. Removal of Zn(II), Cu(II), Ni(II), Ag(I) and Cr(VI) present in aqueous solutions by aluminium electrocoagulation. J. Hazard Mater. 152 (3), 934–941.

Huang, W., Liu, N., Zhang, X., Wu, M., Tang, L., 2017. Metal organic framework g-C_3N_4/MIL-53(Fe) heterojunctions with enhanced photocatalytic activity for Cr(VI) reduction under visible light. Appl. Surf. Sci. 425, 107–116.

Huang, B., Wu, Z., Zhou, H., Li, J., Zhou, C., Xiong, Z., Pan, Z., Yao, G., Lai, B., 2021. Recent advances in single-atom catalysts for advanced oxidation processes in water purification. J. Hazard Mater. 412, 125253.

Karnitz Jr., O., Gurgel, L.V., de Melo, J.C., Botaro, V.R., Melo, T.M., de Freitas Gil, R.P., Gil, L.F., 2007. Adsorption of heavy metal ion from aqueous single metal solution by chemically modified sugarcane bagasse. Bioresour. Technol. 98 (6), 1291–1297.

Kaya, C., Şahbaz, A., Arar, Ö., Yüksel, Ü., Yüksel, M., 2014. Removal of tartaric acid by gel and macroporous ion-exchange resins. Desal. Water Treat 55 (2), 514–521.

Li, Y., Bian, Y., Qin, H., Zhang, Y., Bian, Z., 2017. Photocatalytic reduction behavior of hexavalent chromium on hydroxyl modified titanium dioxide. Appl. Catal. B Environ. 206, 293–299.

Li, Y.-X., Fu, H., Wang, P., Zhao, C., Liu, W., Wang, C.-C., 2019a. Porous tube-like ZnS derived from rod-like ZIF-L for photocatalytic Cr(VI) reduction and organic pollutants degradation. Environ. Pollut. 256, 113417.

Li, P., Guo, M., Wang, Q., Li, Z., Wang, C., Chen, N., Wang, C.-C., Wan, C., Chen, S., 2019b. Controllable synthesis of cerium zirconium oxide nanocomposites and their application for photocatalytic degradation of sulfonamides. Appl. Catal. B Environ. 259, 118107.

Li, Y.-X., Wang, X., Wang, C.-C., Fu, H., Liu, Y., Wang, P., Zhao, C., 2020a. S-TiO_2/UiO-66-NH_2 composite for boosted photocatalytic Cr(VI) reduction and bisphenol A degradation under LED visible light. J. Hazard Mater. 399, 123085.

Li, X.-Y., Rong, H.-P., Zhang, J.-T., Wang, D.-S., Li, Y.-D., 2020b. Modulating the local coordination environment of single-atom catalysts for enhanced catalytic performance. Nano Res. 13 (7), 1842–1855.

Liang, R., Jing, F., Shen, L., Qin, N., Wu, L., 2015. MIL-53(Fe) as a highly efficient bifunctional photocatalyst for the simultaneous reduction of Cr(VI) and oxidation of dyes. J. Hazard Mater. 287, 364–372.

Libenson, G.D.S.M.N., Shakhmin, A.L., 2000. Chemical analysis of products obtained by nanosecond laser ablation. Tech. Phys. 45, 1219–1222.

Liu, A., Wang, C.-Z., Chu, C., Chu, H.-Y., Chen, X., Du, A.-F., Mao, J., Zheng, W., Wang, C.-C., 2018. Adsorption performance toward organic pollutants, odour control and anti-microbial activities of one Ag-based coordination polymer. J. Environ. Chem. Eng. 6 (4), 4961–4969.

Liu, Y., Liu, F., Ding, N., Hu, X., Shen, C., Li, F., Huang, M., Wang, Z., Sand, W., Wang, C.-C., 2020a. Recent advances on electroactive CNT-based membranes for environmental applications: the perfect match of electrochemistry and membrane separation. Chin. Chem. Lett. 31 (10), 2539–2548.

Liu, J., Zhang, X., Zhong, Q., Li, J., Wu, H., Zhang, B., Jin, L., Tao, H.B., Liu, B., 2020b. Electrostatic self-assembly of a AgI/$Bi_2Ga_4O_9$ p–n junction photocatalyst for boosting superoxide radical generation. J. Mater. Chem. 8 (7), 4083–4090.

Liu, X., Liu, G., You, S., 2021. Effective in-situ reduction of Cr(VI) from leather wastewater by advanced reduction process based on $CO_2^{\cdot-}$ with visible-light photocatalyst. Chemosphere 263, 127898.

Lu, Y., Jiang, B., Fang, L., Ling, F., Gao, J., Wu, F., Zhang, X., 2016. High performance NiFe layered double hydroxide for methyl orange dye and Cr(VI) adsorption. Chemosphere 152, 415–422.

Lv, S.-W., Liu, J.-M., Li, C.-Y., Zhao, N., Wang, Z.-H., Wang, S., 2020. In situ growth of benzothiadiazole functionalized UiO-66-NH_2 on carboxyl modified g-C_3N_4 for enhanced photocatalytic degradation of sulfamethoxazole under visible light. Catal. Sci. Technol. 10 (14), 4703–4711.

Milh, H., Yu, X.Y., Cabooter, D., Dewil, R., 2021. Degradation of ciprofloxacin using UV-based advanced removal processes: comparison of persulfate-based advanced oxidation and sulfite-based advanced reduction processes. Sci. Total Environ. 764, 144510.

Nair, V., Panigrahy, A., Vinu, R., 2014. Development of novel chitosan–lignin composites for adsorption of dyes and metal ions from wastewater. Chem. Eng. J. 254, 491–502.

Nie, Y.-C., Yu, F., Wang, L.-C., Xing, Q.-J., Liu, X., Pei, Y., Zou, J.-P., Dai, W.-L., Li, Y., Suib, S.L., 2018. Photocatalytic degradation of organic pollutants coupled with simultaneous photocatalytic H_2 evolution over graphene quantum dots/Mn-N-TiO_2/g-C_3N_4 composite catalysts: performance and mechanism. Appl. Catal. B Environ. 227, 312–321.

Owlad, M., Aroua, M.K., Daud, W.A.W., Baroutian, S., 2009. Removal of hexavalent chromium-contaminated water and wastewater: a review. Water Air Soil Pollut. 200, 59–77.

Peng, Y., Huang, H., Zhang, Y., Kang, C., Chen, S., Song, L., Liu, D., Zhong, C., 2018. A versatile MOF-based trap for heavy metal ion capture and dispersion. Nat. Commun. 9 (1), 187.

Perissinotti, Laura L., Brusa, Marta A., Grela, María A., 2001. Yield of carboxyl anion radicals in the photocatalytic degradation of formate over TiO_2 particles. Langmuir 17 (26), 8422–8427.

Shen, L., Liang, R., Luo, M., Jing, F., Wu, L., 2015. Electronic effects of ligand substitution on metal-organic framework photocatalysts: the case study of UiO-66. Phys. Chem. Chem. Phys. 17 (1), 117–121.

Shen, B., Dong, C., Ji, J., Xing, M., Zhang, J., 2019. Efficient Fe(III)/Fe(II) cycling triggered by MoO_2 in Fenton reaction for the degradation of dye molecules and the reduction of Cr(VI). Chin. Chem. Lett. 30 (12), 2205–2210.

Shi, X., Zhang, X., Bi, F., Zheng, Z., Sheng, L., Xu, J., Wang, Z., Yang, Y., 2020. Effective toluene adsorption over defective UiO-66-NH_2: an experimental and computational exploration. J. Mol. Liq. 316, 113812.

Testa, J.J., Grela, M.A., Litter, M.I., 2004. Heterogeneous photocatalytic reduction of chromium(VI) over TiO_2 particles in the presence of oxalate: Involvement of Cr(V) species. Environ. Sci. Technol. 38 (5), 1589–1594.

Valenzano, L., Civalleri, B., Chavan, S., Bordiga, S., Nilsen, M.H., Jakobsen, S., Lillerud, K.P., Lamberti, C., 2011. Disclosing the complex structure of UiO-66 metal organic framework: a synergic combination of experiment and theory. Chem. Mater. 23 (7), 1700–1718.

Velegraki, G., Miao, J., Drivas, C., Liu, B., Kennou, S., Armatas, G.S., 2018. Fabrication of 3D mesoporous networks of assembled CoO nanoparticles for efficient photocatalytic reduction of aqueous Cr(VI). Appl. Catal. B Environ. 221, 635–644.

Wang, L., Wang, N., Zhu, L., Yu, H., Tang, H., 2008. Photocatalytic reduction of Cr(VI) over different TiO_2 photocatalysts and the effects of dissolved organic species. J. Hazard Mater. 152 (1), 93–99.

Wang, N., Zhu, L., Huang, Y., She, Y., Yu, Y., Tang, H., 2009. Drastically enhanced visible-light photocatalytic degradation of colorless aromatic pollutants over TiO_2 via a charge-transfer-complex path: a correlation between chemical structure and degradation rate of the pollutants. J. Catal. 266 (2), 199–206.

Wang, N., Zhu, L., Deng, K., She, Y., Yu, Y., Tang, H., 2010. Visible light photocatalytic reduction of Cr(VI) on TiO_2 in situ modified with small molecular weight organic acids. Appl. Catal. B Environ. 95 (3–4), 400–407.

Wang, C., Zhu, L., Wei, M., Chen, P., Shan, G., 2012. Photolytic reaction mechanism and impacts of coexisting substances on photodegradation of bisphenol A by Bi_2WO_6 in water. Water Res. 46 (3), 845–853.

Wang, H., Yuan, X., Wu, Y., Zeng, G., Chen, X., Leng, L., Wu, Z., Jiang, L., Li, H., 2015. Facile synthesis of amino-functionalized titanium metal-organic frameworks and their superior visible-light photocatalytic activity for Cr(VI) reduction. J. Hazard Mater. 286, 187–194.

Wang, C.-C., Du, X.-D., Li, J., Guo, X.-X., Wang, P., Zhang, J., 2016a. Photocatalytic Cr (VI) reduction in metal-organic frameworks: a mini-review. Appl. Catal. B Environ. 193, 198–216.

Wang, J.-C., Ren, J., Yao, H.-C., Zhang, L., Wang, J.-S., Zang, S.-Q., Han, L.-F., Li, Z.-J., 2016b. Synergistic photocatalysis of Cr(VI) reduction and 4-Chlorophenol degradation over hydroxylated α-Fe_2O_3 under visible light irradiation. J. Hazard Mater. 311, 11–19.

Wang, F.-X., Yi, X.-H., Wang, C.-C., Deng, J.-G., 2017. Photocatalytic Cr(VI) reduction and organic-pollutant degradation in a stable 2D coordination polymer. Chin. J. Catal. 38 (12), 2141–2149.
Wang, C.-Y., Fu, H., Wang, P., Wang, C.-C., 2019. Highly sensitive and selective detect of *p*-arsanilic acid with a new water-stable europium metal–organic framework. Appl. Organomet. Chem. 33 (8), e5021.
Wang, X.Y., Li, L.Y., Meng, J.Q., Xia, P.Y., Yang, Y.X., Guo, Y.H., 2020. Enhanced simulated sunlight photocatalytic reduction of an aqueous hexavalent chromium over hydroxyl-modified graphitic carbon nitride. Appl. Surf. Sci. 506, 144181.
Wang, X., Li, Y.-X., Yi, X.-H., Zhao, C., Wang, P., Deng, J.G., Wang, C.-C., 2021a. Photocatalytic Cr(VI) elimination over BUC-21/N-$K_2Ti_4O_9$ composites: big differences in performance resulting from small differences in composition. Chin. J. Catal. 42 (2), 259–270.
Wang, J.-W., Qiu, F.-G., Wang, P., Ge, C., Wang, C.-C., 2021b. Boosted bisphenol A and Cr(VI) cleanup over Z-scheme WO_3/MIL-100(Fe) composites under visible light. J. Clean. Prod. 279, 123408.
Wiersum, A.D., Soubeyrand-Lenoir, E., Yang, Q., Moulin, B., Guillerm, V., Yahia, M.B., Bourrelly, S., Vimont, A., Miller, S., Vagner, C., Daturi, M., Clet, G., Serre, C., Maurin, G., Llewellyn, P.L., 2011. An evaluation of UiO-66 for gas-based applications. Chem. Asian J. 6 (12), 3270–3280.
Wu, H., Yildirim, T., Zhou, W., 2013. Exceptional mechanical stability of highly porous zirconium metal-organic framework UiO-66 and its important implications. J. Phys. Chem. Lett. 4 (6), 925–930.
Xie, H., Ma, D., Liu, W., Chen, Q., Zhang, Y., Huang, J., Zhang, H., Jin, Z., Luo, T., Peng, F., 2020. Zr-Based MOFs as new photocatalysts for the rapid reduction of Cr (VI) in water. New J. Chem. 44 (17), 7218–7225.
Xing, Y., Chen, X., Wang, D., 2007. Electrically regenerated ion exchange for removal and recovery of Cr(VI) from wastewater. Environ. Sci. Technol. 41 (4), 1439–1443.
Xiong, Z., Jiang, Y., Wu, Z., Yao, G., Lai, B., 2020. Synthesis strategies and emerging mechanisms of metal-organic frameworks for sulfate radical-based advanced oxidation process: a review. Chem. Eng. J. 127863.
Yang, L., Xiao, Y., Liu, S., Li, Y., Cai, Q., Luo, S., Zeng, G., 2010. Photocatalytic reduction of Cr(VI) on WO_3 doped long TiO_2 nanotube arrays in the presence of citric acid. Appl. Catal. B Environ. 94 (1), 142–149.
Yi, X.-H., Wang, C.-C., 2021. Elimination of emerging organic contaminants in wastewater by advanced oxidation process over iron-based MOFs and their composites. Prog. Chem. 33 (3), 417–489.
Yi, X.-H., Ma, S.-Q., Du, X.-D., Zhao, C., Fu, H., Wang, P., Wang, C.-C., 2019a. The facile fabrication of 2D/3D Z-scheme g-C_3N_4/UiO-66 heterojunction with enhanced photocatalytic Cr(VI) reduction performance under white light. Chem. Eng. J. 375, 121944.
Yi, X.-H., Wang, F.-X., Du, X.-D., Wang, P., Wang, C.-C., 2019b. Facile fabrication of BUC-21/g-C_3N_4 composites and their enhanced photocatalytic Cr(VI) reduction performances under simulated sunlight. Appl. Organomet. Chem. 33 (1), e4621.
Yi, X.-H., Ji, H., Wang, C.-C., Li, Y., Li, Y.-H., Zhao, C., Wang, A., Fu, H., Wang, P., Zhao, X., Liu, W., 2021. Photocatalysis-activated SR-AOP over PDINH/MIL-88A(Fe) composites for boosted chloroquine phosphate degradation: performance, mechanism, pathway and DFT calculations. Appl. Catal. B Environ. 293, 120229.
Yu, H., Shi, R., Zhao, Y., Bian, T., Zhao, Y., Zhou, C., Gin, W., Wu, L.Z., Tung, C.H., Zhang, T., 2017. Alkali-assisted synthesis of nitrogen deficient graphitic carbon nitride with tunable band structures for efficient visible-light-driven hydrogen evolution. Adv. Mater. 29 (16), 1605148–1605154.
Zhang, F., Zhang, Y., Zhou, C., Yang, Z., Xue, H., Dionysiou, D.D., 2017. A new high efficiency visible-light photocatalyst made of SnS_2 and conjugated derivative of polyvinyl alcohol and its application to Cr(VI) reduction. Chem. Eng. J. 324, 140–153.
Zhang, S.-H., Wu, M.-F., Tang, T.-T., Xing, Q.-J., Peng, C.-Q., Li, F., Liu, H., Luo, X.-B., Zou, J.-P., Min, X.-B., Luo, J.-M., 2018a. Mechanism investigation of anoxic Cr(VI) removal by nano zero-valent iron based on XPS analysis in time scale. Chem. Eng. J. 335, 945–953.
Zhang, F., Zhang, Y., Zhang, G., Yang, Z., Dionysiou, D.D., Zhu, A., 2018b. Exceptional synergistic enhancement of the photocatalytic activity of SnS_2 by coupling with polyaniline and N-doped reduced graphene oxide. Appl. Catal. B Environ. 236, 53–63.
Zhang, J., Gao, N., Chen, F., Zhang, T., Zhang, G., Wang, D., Xie, X., Cai, D., Ma, X., Wu, L., Wu, Z., 2019. Improvement of Cr(VI) photoreduction under visible-light by g-C_3N_4 modified by nano-network structured palygorskite. Chem. Eng. J. 358, 398–407.
Zhao, J., Han, Q., Zhu, J., Wu, X., Wang, X., 2014. Synthesis of Bi nanowire networks and their superior photocatalytic activity for Cr(VI) reduction. Nanoscale 6 (17), 10062–10070.
Zhao, C., Wang, Z.H., Li, X., Yi, X.-H., Chu, H.Y., Chen, X., Wang, C.-C., 2020. Facile fabrication of BUC-21/$Bi_{24}O_{31}Br_{10}$ composites for enhanced photocatalytic Cr(VI) reduction under white light. Chem. Eng. J. 389, 123431.
Zhao, C., Wang, J., Chen, X., Wang, Z., Ji, H., Chen, L., Liu, W., Wang, C.-C., 2021. Bifunctional $Bi_{12}O_{17}Cl_2$/MIL-100(Fe) composites toward photocatalytic Cr(VI) sequestration and activation of persulfate for bisphenol A degradation. Sci. Total Environ. 752, 141901.
Zhou, Y.-C., Xu, X.-Y., Wang, P., Fu, H., Zhao, C., Wang, C.-C., 2019. Facile fabrication and enhanced photocatalytic performance of visible light responsive UiO-66-NH_2/Ag_2CO_3 composite. Chin. J. Catal. 40 (12), 1912–1923.
Zhou, Y.-C., Wang, P., Fu, H., Zhao, C., Wang, C.-C., 2020. Ternary Ag/Ag_3PO_4/MIL-125-NH_2 Z-scheme heterojunction for boosted photocatalytic Cr(VI) cleanup under visible light. Chin. Chem. Lett. 31 (10), 2645–2650.
Zou, J.-P., Wu, D.-D., Luo, J., Xing, Q.-J., Luo, X.-B., Dong, W.-H., Luo, S.-L., Du, H.-M., Suib, S.L., 2016. A strategy for one-pot conversion of organic pollutants into useful hydrocarbons through coupling photodegradation of MB with photoreduction of CO_2. ACS Catal. 6 (10), 6861–6867.